RSC Advances

PAPER

View Article Online
View Journal | View Issue



Cite this: *RSC Adv.*, 2023, **13**, 15531

# Citric acid modified semi-embedded silver nanowires/colorless polyimide transparent conductive substrates for efficient flexible perovskite solar cells†

Jie Gong, *[ab] Xiao Fan,[a] Zhangyang Zong,[a] Mingyang Yang,[a] Ya Sun[a] and Guoqun Zhao *[b]

Flexible solar cells, with the merits of structure compactness and shape transformation, are promising power sources for future electronic devices. However, frangible indium tin oxide-based transparent conductive substrates severely limit the flexibility of solar cells. Herein, we develop a flexible transparent conductive substrate of silver nanowires semi-embedded in colorless polyimide (denoted as AgNWs/cPI) *via* a simple and effective substrate transfer method. A homogeneous and well-connected AgNW conductive network can be constructed through modulating the silver nanowire suspension with citric acid. As a result, the prepared AgNWs/cPI shows low sheet resistance of about 21.3 ohm sq.$^{-1}$, high transmittance at 550 nm of 94%, and smooth morphology with the peak-to-valley roughness value of 6.5 nm. The perovskite solar cells (PSCs) on AgNWs/cPI exhibit power conversion efficiency of 14.98% with negligible hysteresis. Moreover, the fabricated PSCs maintain nearly 90% initial efficiency after bending for 2000 cycles. This study sheds light on the importance of suspension modification for the distribution and connection of AgNWs and paves a way for the development of high-performance flexible PSCs for practical applications.

Received 13th March 2023
Accepted 18th May 2023

DOI: 10.1039/d3ra01639k

rsc.li/rsc-advances



## 1. Introduction

Flexible solar cells are promising power sources for wearable and portable electronic devices due to their compact structure and transformable shape. Perovskite solar cells (PSCs) in particular are desirable candidates for flexible photovoltaics because of their high power conversion efficiency (PCE), low-temperature solution processability and outstanding flexibility.[1–6] However, practical applications have raised higher expectations for flexible electronics that must withstand thousands of bends and even folds with extreme radius of curvature, which makes widely used indium tin oxide (ITO)-based transparent electrodes unsatisfactory due to their inherent brittleness, poor mechanical flexibility, and high material cost.[7–9]

The drawbacks of ITO have promoted the search for alternative flexible transparent conductive films. Among the various flexible transparent conductive films available, such as carbon nanotube,[10,11] graphene,[12,13] conductive polymer and metallic nanowires,[14–17] silver nanowires (AgNWs)-based transparent conductive films have been regarded as the most promising candidates due to their low sheet resistance, high transmittance, excellent mechanical flexibility and solution processability.[18–20] However, AgNWs-based transparent conductive films still suffer from high surface roughness caused by the random distribution and overlapping of AgNWs in their films, which can lead to device performance degradation or even device short circuit.[21,22] Moreover, there are concerns that the disconnected nanowires may impede charge transportation and thus affect device performances.[23] Besides, the noble metal coverage will increase overall cost, thus strategies to improve the performance of transparent electrodes while maintaining the amount of usage of noble metal should be a focus for further application.[24,25] To address these issues, several methods have been proposed, such as mechanical pressing with tens of MPa pressure,[26] spray coating at a direct current electric field and plasma treatment,[27] filling the AgNWs with polymer,[28] and so on. Wan *et al.*[27] reported a low direct current electric field spray coating strategy and plasma post treatment to improve the arrangement and surface roughness of AgNWs. For practical applications, it is highly desirable for a simple and low equipment-required strategy to realize the homogeneous-distributed and well-connected AgNWs.

[a]*China Aerospace Science & Industry Corp. (Changsha) Advanced Material Research Institute Co., Ltd, Changsha, Hunan 410205, PR China. E-mail: gongjie_@mail.sdu.edu.cn*

[b]*Key Laboratory for Liquid-Solid Structural Evolution and Processing of Materials, Ministry of Education, Shandong University, Jinan, Shandong 250061, PR China. E-mail: zhaogq@sdu.edu.cn*

† Electronic supplementary information (ESI) available. See DOI: https://doi.org/10.1039/d3ra01639k

The most commonly used flexible substrates to provide support for AgNWs include polydimethylsiloxane (PDMS),[29] polymethyl methacrylate (PMMA),[30] polyethylene terephthalate (PET),[31] colorless polyimide (cPI),[32,33] *etc.* Among these substrates, cPI has been the most promising candidate due to its excellent thermal stability, high optical transparency, and great flexibility.[34,35] In particular, the substrates of AgNWs semi-embedded in cPI (denoted as AgNWs/cPI) have been applied as the transparent conductive substrates in flexible electronics.[36,37] Miao *et al.*[37] achieved a PCE of 11.8% through fabricating flexible PSCs on AgNWs/cPI substrate, and demonstrated an excellent foldable stability with 73.5% and 55.2% of the initial PCE after +180° and −180° folding for 1000 cycles, respectively. However, the issues of inhomogeneous distribution and overlapping of AgNWs, enabling the relatively low optical transmittance and poor roughness, which seriously affects the performance of flexible PSCs.

In this study, a facile and effective strategy is developed to prepare a high-performance flexible AgNWs/cPI transparent conductive substrate with uniform and well-connected AgNWs networks which is achieved through manipulating the sliver nanowires suspension with citric acid (CA). Although AgNWs-based and/or AgNWs/cPI-based composites for various flexible functional applications have been extensively studied.[38–43] The added advantage of our approach is that the CA modulation of AgNWs suspension can improve the distribution uniformity and interconnection of AgNWs conductive network which semi-embedded in the cPI film. The resulting flexible AgNWs/cPI exhibits features of encouraging electro-optical property (low sheet resistance of about 21.3 ohm sq.$^{-1}$ with high transmittance at 550 nm ($T_{550}$) of 94%) and smooth morphology (peak-to-valley roughness of 6.5). PSCs are fabricated using the prepared flexible AgNWs/cPI as transparent conductive substrate, achieving a high PCE of 14.98% with negligible hysteresis. In addition, the fabricated PSCs show excellent stability applied with continuous mechanical bending (nearly 90% initial efficiency maintained after 2000 cycles). This development of flexible AgNWs/cPI is promising for constructing high-performance, easily fabricated, and low-cost ITO-free PSCs, paving the way for further improvements in the mechanical stability of flexible electronic devices.

## 2. Experimental

### 2.1 Preparation of flexible AgNWs/cPI

AgNWs suspensions (10 mg ml$^{-1}$) in ethanol with an average wire diameter of 30 nm and average wire lengths of 20 μm or 100 μm were purchased from Guangzhou Nano Chemical Technology Co., Ltd. CPI was provided by Zhejiang Daoming Optics & Chemical Co., Ltd. First, the glass supporters were cleaned using sequential ultrasonication in detergent (purchased from Shenzhen Ruigeruisi Technology Co., Ltd), de-ionized water, and ethanol (purchased from Sinopharm Chemical Reagent Co., Ltd) for 30 min, respectively. The cleaned glass supporters were treated with plasma for 20 min before use. Next, for preparing AgNWs suspension with CA, 10 mg CA (AR, purchased from Sinopharm Chemical Reagent Co., Ltd) was dissolved in 8 ml ethanol in an ultrasonic bath for 2 min. And 2 ml of the purchased AgNWs suspension was added into the ethanol solution of CA drop by drop with continuous mixing. For comparison, the AgNWs suspension without CA was prepared by diluting the purchased AgNWs suspension directly with ethanol. Then, 60 μl AgNWs suspension was spin-coated onto a cleaned glass supporter at 2000 rpm and 1 min for 2 layers, and heated on a hot plate at 120 °C for 10 min. Next, selectively patterning of the AgNWs layer can be enabled by knife etching. After that, cPI in dimethylformamide (DMAc, AR, purchased from Sinopharm Chemical Reagent Co., Ltd) solution (20 wt%) was spin-coated at 1000 rpm for 30 s on the AgNWs layer. Immediately, the composite sample was cured by a gradient heating process, which performed with a heating rate of 1 °C min$^{-1}$ to reach 80, 110, 140, and 170 °C and hold for 1 h each step. The temperature–time curve in gradient heating process is shown in Fig. S1.† Right after the heating process, the sample were cooled down in the furnace. Finally, the slowly cool-downed AgNWs/cPI was peeled off from the glass supporter by soaking in water.

### 2.2 Fabrication of flexible PSCs

The AgNWs/cPI peeled off was dried at 60 °C for 12 h. And the PEDOT:PSS AI 4083 mixed with different volumes of $NiO_x$ solution was spin-coated onto the AgNWs/cPI substrate at 3000 rpm for 1 min and annealed at 100 °C for 20 min. The preparation of $NiO_x$ solution was referred to previous report.[44] After cooling, the mixed-cation perovskite film was then deposited by one-step spin-coating. The 1.7 M perovskite precursor solution was prepared by mixing CsI, FAI, MABr, $PbI_2$ and $PbBr_2$ with a formula of $Cs_{0.05}(FA_{0.98}MA_{0.02})_{0.95}Pb(I_{0.98}Br_{0.02})_3$ in DMF/DMSO (4/1 vol). The 10 mol% of MACl and 0.6 mol% ODADI were added into the perovskite precursor. 60 μl perovskite precursor solution was spin-coated at 1000 rpm for 10 s and 5000 rpm for 45 s. During the second step, 180 μl chlorobenzene (CB) as anti-solvent was dripped onto the center of perovskite film for 12 s before the end of spin-coating. The as-deposited films were transferred to a vacuum chamber with a negative pressure 0.1 MPa for pretreatment to evaporate most of the solvent in the film, and then annealed at 100 °C for 30 min. The spin-coating processes were all conducted at room temperature in $N_2$. In the end, 25 nm $C_{60}$, 6 nm BCP and 100 nm silver electrode were subsequently thermal evaporated under high vacuum (<5 × 10$^{-6}$ Torr).

### 2.3 Characterization

The sheet resistance of the samples was determined by a four-point probe system (SZT-2C, China). Transmittance was recorded using a UV-vis spectrophotometer (TU-1810, China). Since the use of glass as supporter for AgNWs deposition, the transmittance of the AgNWs film was calculated by subtracting the transmittance curve of the glass supporter from the transmittance curve of the AgNWs/glass sample. While the reference of self-supported pure cPI, AgNWs/cPI and ITO–PET samples is air. Scanning electron microscopy (SEM) images of the samples were characterized by utilizing Tescan Amber GMH field-

 

emission double-beam scanning electron microscope. Surface roughness was analyzed using atomic force microscope (AFM, Dimension Icon). Photovoltaic performance measurements of solar cells were performed in $N_2$ at room temperature by using a Keithley 2400 SourceMeter under simulated sunlight with a solar simulator (EnliTech, SS-F5, Taiwan). A National Renewable Energy Laboratory calibrated standard silicon cell (with a KG-2 filter) was used to obtain the AM 1.5G (100 mW $cm^{-2}$) solar light intensity. The flexible PSCs were covered by using a metal mask with aperture area of 0.04 $cm^2$. The *J–V* measurements was carried out using sweep mode under reverse (1.20 V to −0.01 V) and forward (−0.01 V to 1.20 V) scan with a rate of 10 mV $s^{-1}$.

## 3. Results and discussion

The schematic diagram of the preparation of flexible AgNWs/cPIs is depicted in Fig. 1a. Briefly, AgNWs suspension without or with CA is first spin-coated on a glass substrate, respectively. Then, cPI solution is spin-coated onto the AgNWs film. After gradient heating, the flexible AgNWs/cPI is obtained by peeing off from the glass. It should be noticed that for selecting the spin-coating process parameters of AgNWs suspension, AgNWs/glass samples prepared with different lengths (20 or 100 μm) are studied by varying the AgNWs suspension dilution ratio and the spin-coating layer. The detailed sheet resistance of AgNWs/glass samples are summarized in ESI Fig. S2 and Table S1.† The visible light transmittance and $T_{550}$ of AgNWs/glass samples are shown in ESI Fig. S3, S4 and Table S2,† respectively. The transmittance has a trade-off relationship with the electrical conductivity. As the adhesion amount of the AgNWs coated on a glass substrate increased, the transmittance decreased, corresponding to a decrease in the sheet resistance.[45]

The relationship between sheet resistance and $T_{550}$ of AgNWs/glass samples with 20 μm or 100 μm lengths are shown in ESI Fig. S5.† It is shown that the samples with longer length of AgNWs (100 μm) possess higher optical-electrical characteristic. Hereafter, for further investigation, we chose AgNWs with 100 μm length for fabricating the AgNWs/glass and AgNWs/cPI samples with/without CA, as well as the solar cells. From the sheet resistance of AgNWs/glass samples shown in ESI Fig. S2 and Table S1,† it can be seen that when the dilution ratio is 1 : 4 and the number of spin-coating layer is 2, the sheet resistance value of the AgNWs network (39.0 ± 3.94 ohm $sq.^{-1}$) is close to the sheet resistance value of ITO–PET (42.9 ± 2.07 ohm $sq.^{-1}$). For better comparison, this process condition serves as representative case for deposition. The sheet resistance and $T_{550}$ of the selected AgNWs/glass sample are about 39.0 ± 3.94 ohm

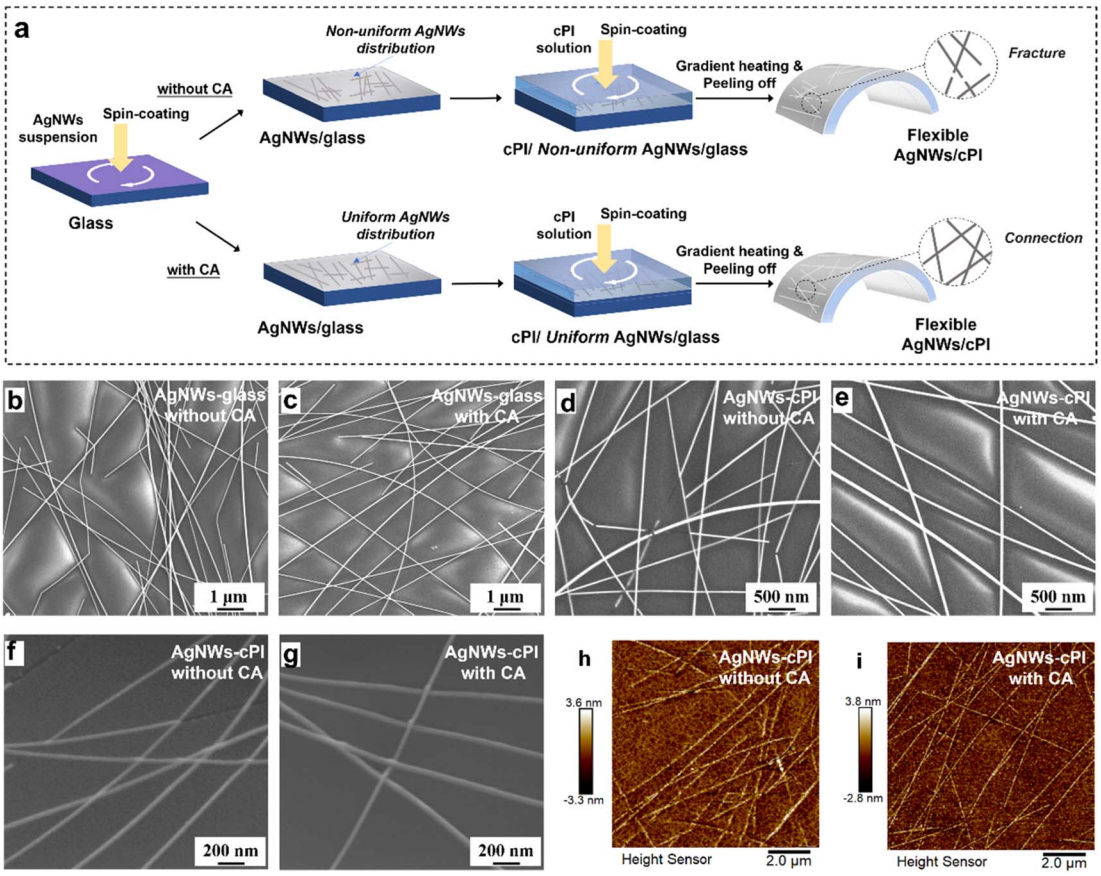


Fig. 1 (a) Schematic diagram of the preparation of flexible AgNWs/cPIs. SEM images of the surface of AgNWs/glass samples prepared without (b) or with (c) CA. SEM images of the surface of flexible AgNWs/cPI samples prepared without (d) or with (e) CA. 60° titled SEM images of the surface of flexible AgNWs/cPI samples prepared without (f) or with (g) CA. AFM images of the flexible AgNWs/cPI samples prepared without (h) or with (i) CA.

sq.$^{-1}$ and 97.6%, respectively. In addition, as shown in ESI Fig. S6,† the pure cPI flexible substrate (about 20 μm thick) shows high transmittance of >94% at the visible light region, with a $T_{550}$ of 96.9%.

The scanning electron microscopy (SEM) images of the surface of AgNWs/glass samples prepared without or with CA are shown in Fig. 1b, c and ESI Fig. S7.† The AgNWs network prepared from AgNWs suspension lacking CA exhibits a considerably aggregated structure. In contrast, the AgNWs network prepared from AgNWs suspension with CA demonstrates a well-distributed structure without aggregations. The SEM images of the samples with different CA content are shown in ESI Fig. S8.† We can see that the AgNWs distribution could be improved with the increase of CA amount. It might be attributed to the formation of hydrogen bonds between the carboxyl acid group of CA and the amide group of polyvinyl pyrrolidone on the surface of AgNWs, which prevents an aggregation of AgNWs network.[46] We have to state that the AgNWs products were synthesized by a polyol method. In the synthesis of AgNWs, a fixed amount of PVP should be employed as the capping agent to control nanostructure size.[47,48] The presence of PVP layer on the surface of AgNWs has been widely proven. PVP generally decomposes at about 300 °C, and can be removed above 500 °C.[49] It should be noted that the sheet resistances of AgNWs/glass samples fabricated with different amounts of CA are tested. Compared to the AgNWs/glass sample without CA (ESI Table S3†), increasing the concentration of CA tends to reduce the sheet resistance, which could be ascribed to the improved AgNWs distribution. When the CA concentration is 1 mg ml$^{-1}$, the sheet resistance value of AgNWs/glass sample is the lowest. Further increasing the CA concentration to 1.5 mg ml$^{-1}$ or 2 mg ml$^{-1}$ causes a higher sheet resistance owing to the natural non-conductive nature of CA.

The SEM images and the 60° titled SEM images of the surface of flexible AgNWs/cPI samples prepared without or with CA are shown in Fig. 1d–g. The AgNWs network exhibits no clear damage prepared with CA. While the AgNWs network are broken without the addition of CA. ESI Table S4† shows that the sheet resistances of AgNWs/cPI products prepared with CA are lower than those of AgNWs/cPI products prepared without CA under different gradient heating conditions. The reasons that CA protects AgNWs from breaking might be explained in two ways. On the one hand, CA forms a protective layer on the surface of AgNWs, which can release the high temperature fusing phenomenon of AgNWs.[50] On the other hand, the addition of CA improves the distribution uniformity of AgNWs, which is beneficial to improve the uniformity of heat distribution during gradient heating.[23]

The atomic force microscope (AFM) images of Fig. 1h and i show that the AgNWs are semi-embedded in cPI through using the simple substrate transfer method, which is consistent with the results displayed in the SEM images of Fig. 1f and g. The AgNWs/cPI film with CA treatment shows a more uniform distribution compared to the sample without CA. As shown in ESI Fig. S9,† the roughness of the flexible AgNWs/cPI products prepared without (peak-to-valley roughness of 7.2) or with (peak-to-valley roughness of 6.5) CA are lower than that of commercial ITO–PET (peak-to-valley roughness of 17.3). The high smoothness of the flexible AgNWs/cPI samples could be attributed to the peel-off technology which has the advantages of an effective removal of the AgNWs/cPI film from the supporting glass by the moisture-induced adhesion degradation and strong interaction between the conductive AgNWs layer and *in situ* film formed cPI.[51]

Fig. 2a shows the transmittance of the flexible AgNWs/cPI samples prepared without or with CA and commercial ITO–PET film. The transmittance of AgNWs/cPI prepared with CA is higher than that of the commercial ITO–PET film at the visible light region, while the transmittance is less influenced by CA. The figure of merit (FOM) is popularly used to evaluate the optical-electrical properties of transparent conductive electrodes, as follow:[20,52]

$$\mathrm{FOM} = \frac{188.5}{R_{\mathrm{sh}}\left(\frac{1}{\sqrt{T}} - 1\right)} \quad (1)$$

where $R_{\mathrm{sh}}$ is the sheet resistance, $T$ is the transmittance of a wavelength of 550 nm. The AgNWs/cPI sample prepared with CA has a high $T_{550}$ of 94% and a low sheet resistance of about 21.3 ohm sq.$^{-1}$ (see in Fig. 2b), bring a high FOM of 281.6. The FOM of AgNWs/cPI sample prepared with CA is higher than those of the AgNWs/cPI sample prepared without CA (63.9) and

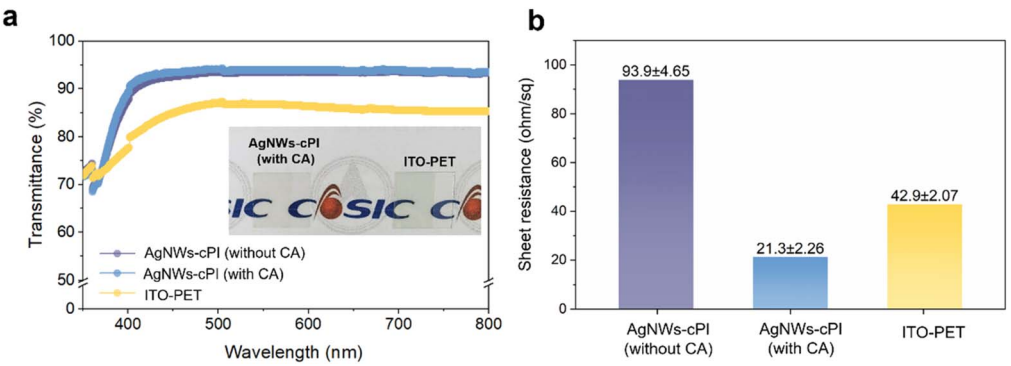


Fig. 2 (a) Transmittance (air as reference) and (b) sheet resistance of the flexible AgNWs/cPI samples prepared without or with CA and commercial ITO–PET (insert photograph shows the flexible AgNWs/cPI sample prepared with CA and ITO–PET as a comparison).

Table 1 Sheet resistance, transmittance at 550 nm (air as reference), and FOM value of the AgNWs/cPI prepared with CA and comparison with previously reported AgNWs (or their composite)/cPI transparent electrodes. The FOM value of AgNWs/cPI reported here, is better than those from literatures

| Deposition method | Electrode structure | Sheet resistance (ohm sq.$^{-1}$) | Transmittance at 550 nm (%) | FOM value |
|---|---|---|---|---|
| Citric acid modified spin coating | AgNWs/cPI (this work) | 21.3 ± 2.26 | 94 | 281.6 |
| Spin coating | AgNWs/cPI[51] | 53.6 | 96 | 171 |
| $SnO_2$ modified spin coating | AgNWs/$SnO_2$/cPI[52] | 9.6 | 86.7 | 265 |
| Spray coating | AgNWs/cPI[53] | 3.6 | 70 | 268 |
| Drop coating | AgNWs/cPI[20] | 20 | 85 | 111 |
| Road coating | AgNWs/cPI[37] | 17.9 | 81.9 | 100 |
| $TiO_x$ modified spin coating | AgNWs/$TiO_x$/cPI[54] | 8 | 79 | 188 |
| | | 10 | 82 | 181 |
| | | 20 | 90 | 174 |
| Spin coating | AgNWs/cPI[22] | 24.4 | 83.2 | 80 |
| Spin coating | AgNWs/cPI[32] | 12.7 | 86.3 | 194 |

commercial ITO–PET film (60.9). Moreover, as tabulated in Table 1, the FOM value of AgNWs/cPI sample with CA is better than those previously reported AgNWs (or their composite)/cPI transparent electrodes.[20,22,32,37,51–54] These results indicate the addition of CA is a highly effective approach for the preparation of AgNWs/cPI substrates with improved distribution uniformity and prevention of nanowire breakage, thus providing enhanced conductivity without significant degradation of transmittance.

To estimate the performance of flexile AgNWs/cPI substrates on the photovoltaic devices, as shown in Fig. 3a, we fabricate flexible inverted PSCs with a device structure of cPI/AgNWs/poly(3,4-ethylenedioxythiophene):poly(styrene sulfonate) (PEDOT:PSS)–$NiO_x$/perovskite/fullerene ($C_{60}$)/2,9-dimethyl-4,7-diphenyl-1,10 phenanthroline (BCP)/silver (Ag). The choice of hole transport layer refers to the previous research of flexible PSCs on Ag-mesh substrate,[44] and the ratio of PEDOT:PSS and $NiO_x$ has been modulated for optimal photovoltaic performance (as shown in ESI Fig. S10†). The current–voltage ($J$–$V$) curves of the best-performing flexible PSCs based on AgNWs/cPI substrates are shown in Fig. 3b. The PSC fabricated on AgNWs/cPI without CA exhibits a highest PCE of 11.55%, with an open-circuit voltage ($V_{OC}$) of 1.000 V, a short-circuit current density ($J_{SC}$) of 20.81 mA cm$^{-2}$ and a fill factor (FF) of 55.51%. After introducing CA into AgNWs/cPI, the device exhibits a significantly improved PCE to 14.98%, with a $V_{OC}$ of 1.052 V, a $J_{SC}$ of 21.23 mA cm$^{-2}$ and an FF of 67.08%. The photovoltaic parameters of flexible solar cells on AgNWs-based/polymer transparent conductive electrodes measured under solar simulator AM 1.5G illumination are tabulated in Table 2. The

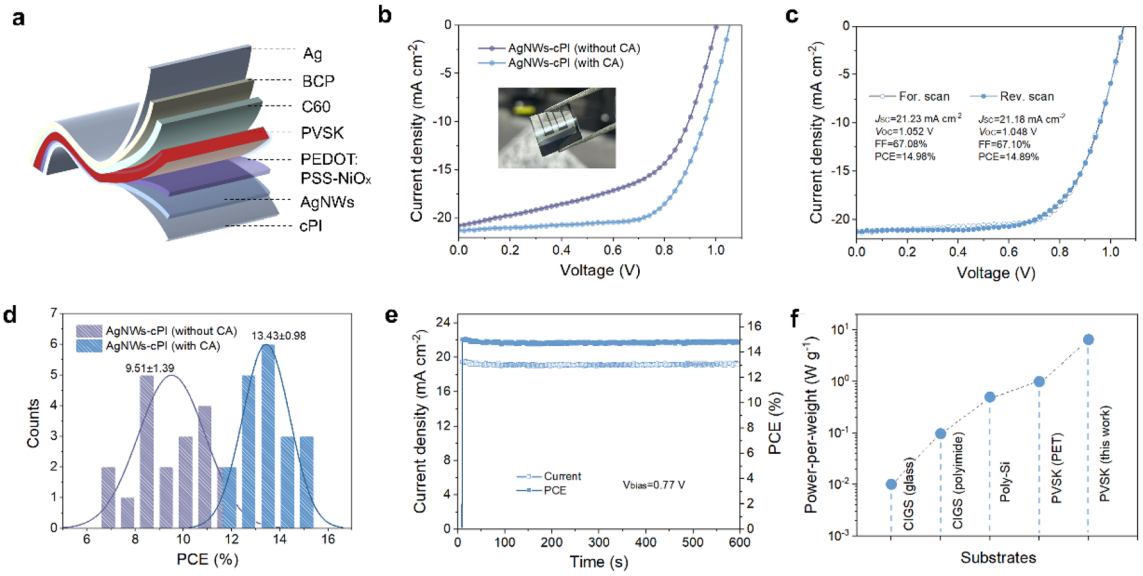


Fig. 3 (a) Schematic illustration of flexible PSCs fabricated on AgNWs/cPI substrate. (b) $J$–$V$ curves of the best performing flexible PSCs based on AgNWs/cPI substrate without and with CA. (c) $J$–$V$ curve of the best performing flexible PSCs based on AgNWs/cPI substrate with CA under forward and reverse scan. (d) Statistics of PCE distribution for flexible PSCs based on AgNWs/cPI substrate without and with CA. (e) Stabilized current and efficiency of best performing flexible PSCs under continuous illumination. (f) Comparison of the power-per-weight of several photovoltaic devices.

Table 2 Comparison of the photovoltaic parameters of flexible solar cells on AgNWs-based/polymer transparent conductive electrodes measured under solar simulator AM 1.5G illumination

| Type of solar cell | Electrode structure | $V_{OC}$ (V) | $J_{SC}$ (mA cm$^{-2}$) | FF (%) | PCE (%) |
|---|---|---|---|---|---|
| Perovskite solar cells (this work) | AgNWs/cPI | 1.052 | 21.23 | 67.08 | 14.98 |
| Perovskite solar cells[37] | AgNWs–ITO/cPI | 1.07 | 17.8 | 62.3 | 11.9 |
| Perovskite solar cells[55] | AgNWs–graphene/PET | 0.956 | 16.48 | 61.8 | 9.73 |
| Perovskite solar cells[56] | AgNWs–PH1000/PLA | 0.91 | 18.79 | 67 | 11.44 |
| Perovskite solar cells[57] | AgNWs–ZnO–$TiO_2$/PET | 1.03 | 22.45 | 74 | 17.11 |
| Perovskite solar cells[58] | AgNWs–chitosan/PEN | 1.04 | 21 | 36.1 | 7.9 |
| Organic solar cells[23] | AgNWs–PEDOT:PSS/cPI | 0.83 | 26.03 | 70 | 15.12 |
| Organic solar cells[59] | AgNWs/cPI | 0.79 | 10.21 | 48.4 | 3.88 |
| Organic solar cells[32] | AgNWs/cPI | 0.78 | 24.77 | 74.35 | 14.37 |
| Organic solar cells[20] | AgNWs/cPI | 0.75 | 12.21 | 43.6 | 4.01 |
| Organic solar cells[22] | AgNWs/cPI | 0.82 | 19.6 | 72 | 11.6 |

flexible PSCs based on AgNWs/cPI substrates with CA in this work show excellent photovoltaic performances among the available literatures so far.[20,22,23,32,37,55–59]

Fig. 3c shows the *J*–*V* curves of the best-performance flexible PSCs based on AgNWs/cPI substrates under forward and reverse scanning. The PCEs obtained under forward and reverse scan are 14.98% and 14.89%, respectively, manifesting a negligible hysteresis, which is also demonstrated in the devices without CA treatment in ESI Fig. S11.† Fig. 3d shows the PCE statistics of the AgNWs/cPI-based flexible PSCs in 20 individual devices, where the average PCE is 13.43 ± 0.98% and 9.51 ± 1.39% for devices with and without CA, respectively. Moreover, a stabilized photocurrent of 19.28 mA cm$^{-2}$ and corresponding PCE of 14.84% are achieved for the best performing device at the maximum power point (MPP) (Fig. 3e).

Lightweight is an advantage of cPI, and to demonstrate this feature, we compare the power-per-weight value of our devices with the typical photovoltaic devices, as shown in Fig. 3f. It is noteworthy that the power-per-weight of the AgNWs/cPI-based flexible PSCs is approximately 6.45 W g$^{-1}$ (with a weight of 4.7 mg), which is higher than that of the commercial ITO–PET-based devices fabricated by ourselves (about 1.05 W g$^{-1}$ with a weight of 38.5 mg, see in ESI Fig. S12†) and significantly superior to most of traditional photovoltaic devices.[60] In addition to the photovoltaic performance, we also evaluate the light and heat stability of the flexible PSCs through recording the efficiency evolution under continuous light conditions (AM 1.5G simulated sunlight) and 85 °C heating, respectively, as shown in ESI Fig. S13 and S14.† The devices fabricated on AgNWs/cPI substrates exhibit similar efficiency decay to the ITO–PET substrate, indicating excellent stability and effective blocking of the hole transport layer to prevent the reaction of perovskite and AgNWs.

Considering that flexible PSCs need to be bent or even folded in practical applications, several tests are conducted to assess the resistance variation of AgNWs/cPI and ITO–PET substrates under different mechanical stresses such as folding, twisting, and extreme crumpling, as illustrated in Fig. 4a. Folding and twisting treatments have negligible effects on AgNWs/cPI substrates, while increasing the sheet resistance of ITO–PET substrates by 1.5 and 7.1 times, which can be attributed to the fragmentation of ITO under stress. Remarkably, even after the crumpling treatment, the AgNWs/cPI with CA maintains almost unchanged sheet resistance, demonstrating the suitability of flexible cPI and bendable AgNWs for flexible electronics under extreme mechanical conditions. On the contrary, the AgNWs/cPI without CA exhibits slightly increased sheet resistance value, which may be due to that the AgNWs with poorer connectivity are more vulnerable to damage when crumpled.

Fig. 4b presents the PCE variations under mechanical bending applied to flexible PSCs with different curvature radius. As the bending radius gradually decreases to 4 mm, there is no obvious efficiency drop for all flexible devices. Further reducing the bending radius to 2 mm, the performance of the AgNWs/cPI-based device is slightly higher than that of the ITO–PET-based device, although the efficiencies of all devices drop significantly. This attenuation could come from cracks and collapses of the perovskite film. In order to verify the real bending performance of the flexible substrate to exclude the influence of perovskite, we conduct a total of 2000 continuous bending fatigue experiments with a radius of 4 mm on the automatic mechanical device (ESI Fig. S15†). The average sheet resistance of AgNWs/cPI with CA, AgNWs/cPI without CA, and ITO–PET increase by 1.07, 1.25, and 10 times, corresponding to $R_0/R$ of 0.931 ± 0.013, 0.797 ± 0.035, and 0.099 ± 0.026, respectively. These results further demonstrate the superior mechanical bending capabilities of the flexible AgNWs/cPI film.

To examine the performance of flexible substrates after bending tests, we fabricate PSCs on the tested flexible substrates and evaluate their photovoltaic performance. As shown in Fig. 4d, despite a modest rise in AgNWs/cPI sheet resistance, the performance of PSCs shows not significantly impacted. Conversely, PSCs fabricated on the ITO–PET substrate represent a relatively noticeable decline in performance due to the increase in ITO resistance and the deformation of PET substrate. In addition, the PCE evolution of flexible PSCs prepared on different substrates under multiple bending cycles is shown in Fig. 4e. The PSCs based on AgNWs/cPI with CA exhibit the best mechanical stability with nearly 90% initial efficiency maintained after 2000 cycles. The photovoltaic performance of PSCs fabricated on AgNWs/cPI without CA drops below 80% after 2000 cycles. The performance of PSCs

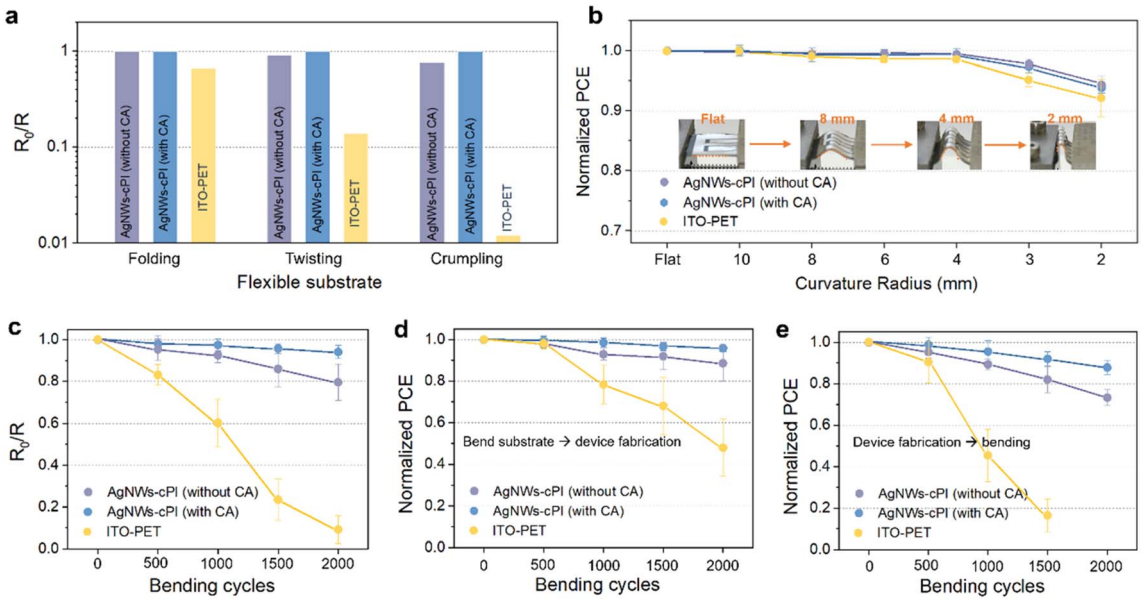


Fig. 4 (a) Sheet resistance variation of the flexible substrate under bending, twisting and crumpling, respectively. $R_0$ and $R$ represent the sheet resistance before and after treatment. (b) PCE variation of flexible PSCs during mechanical bending test with different curvature radius. (c) Sheet resistance variation of the flexible substrate tested under different bending cycles at a curvature radius of 4 mm. (d) PCE of flexible PSCs fabricated on the substrates that have been bend tested. (e) PCE variation of flexible PSCs tested under different bending cycles at a curvature radius of 4 mm.

fabricated on ITO–PET declines more rapidly, falling below 20% after 1500 cycles. These outcomes reinforce the superior mechanical stability of the CA-modified flexible AgNWs/cPI substrates, rendering them suitable for flexible electronics in more challenging application scenarios.

## 4. Conclusions

In summary, we developed a facile and efficient strategy to fabricate flexible AgNWs/cPI transparent conductive substrates for flexible PSCs. The introduction of CA into the AgNWs suspension can improve the distribution uniformity and interconnection of AgNWs semi-embedded in the cPI film, which enables the flexible AgNWs/cPI to exhibit excellent electrical conductivity (low sheet resistance of about 21.3 ohm sq.$^{-1}$), high transmittance (94% of $T_{550}$) and smooth morphology (peak-to-valley roughness of 6.5 nm). The PSCs fabricated using CA treated AgNWs/cPI achieve a champion PCE of 14.98% with negligible hysteresis. Moreover, the fabricated device shows excellent mechanical bending stability, with nearly 90% initial efficiency maintained after 2000 cycles. This work highlights the significance of suspension modification for the AgNWs distribution and connection in AgNWs/cPI flexible conductive substrates, providing theoretical guidance for improving the performance and mechanical stability of AgNWs-based flexible electronic devices.

## Author contributions

Jie Gong: conceptualization, methodology, investigation and writing-original draft; Guoqun Zhao and Xiao Fan: conceptualization, supervision, writing-review & editing, funding acquisition; Zhangyang Zong, Mingyang Yang and Ya Sun: investigation & improving the manuscript.

## Conflicts of interest

There are no conflicts to declare.

## Acknowledgements

The authors acknowledge the support at the Post-Doctoral Research Center at China Aerospace Science & Industry Corp. (Changsha) Advanced Material Research Institute Co., Ltd, and the Key Research and Development Program of Shandong Province of China (Grant No. 2021ZLGX01).

## Notes and references

1 M. Jeong, I. W. Choi, E. M. Go, Y. Cho, M. Kim, B. Lee, S. Jeong, Y. Jo, H. W. Choi, J. Lee, J. Bae, S. K. Kwak, D. S. Kim and C. Yang, *Science*, 2020, **369**, 1615–1620.
2 J. Xue, R. Wang, X. Chen, C. Yao, X. Jin, K. Wang, W. Huang, T. Huang, Y. Zhao, Y. Zhai, D. Meng, S. Tan, R. Liu, Z. Wang, C. Zhu, K. Zhu, M. C. Beard, Y. Yan and Y. Yang, *Science*, 2021, **371**, 636–640.
3 J. J. Yoo, G. Seo, M. R. Chua, T. G. Park, Y. Lu, F. Rotermund, Y. Kim, C. S. Moon, N. J. Jeon, J. Correa-Baena, V. Bulović, S. S. Shin, M. G. Bawendi and J. Seo, *Nature*, 2021, **590**, 587–593.
4 Z. Li, B. Li, X. Wu, S. A. Sheppard, S. Zhang, D. Gao, N. J. Long and Z. Zhu, *Science*, 2022, **376**, 416–420.

5 D. Gao, B. Li, Z. Li, X. Wu, S. Zhang, D. Zhao, X. Jiang, C. Zhang, Y. Wang, Z. Li, N. Li, S. Xiao, W. C. H. Choy, A. K.-Y. Jen, S. Yang and Z. Zhu, *Adv. Mater.*, 2023, **35**, 2206387.
6 Z. Li, X. Wu, B. Li, S. Zhang, D. Gao, Y. Liu, X. Li, N. Zhang, X. Hu, C. Zhi, A. K.-Y. Jen and Z. Zhu, *Adv. Energy Mater.*, 2021, **12**, 2103236.
7 D. Kim, J. W. Han, K. T. Lim and Y. H. Kim, *ACS Appl. Mater. Interfaces*, 2018, **10**, 985–991.
8 Y. Gao, K. Huang, C. Long, Y. Ding, J. Chang, D. Zhang, L. Etgar, M. Liu, J. Zhang and J. Yang, *ACS Energy Lett.*, 2022, **7**, 1412–1445.
9 Y. Peng, B. Du, X. Xu, J. Yang, J. Lin and C. Ma, *Appl. Phys. Express*, 2019, **12**, 066503.
10 Z. Zhang, W. Yan, Y. Chen, S. Chen, G. Jia, J. Sheng, S. Zhu, Z. Xu, X. Zhang and Y. Li, *ACS Nano*, 2022, **16**(1), 1063–1071.
11 H. Yao, L. Ye, H. Zhang, S. Li, S. Zhang and J. Hou, *Chem. Rev.*, 2016, **116**, 7397–7457.
12 R. Zhang, Y. Liao, Y. Zhou and J. Qian, *J. Nanopart. Res.*, 2020, **22**, 39.
13 T. Wang, Y.-Z. Wang, L.-C. Jing, Q. Zhu, A. S. Ethiraj, W. Geng, Y. Tian, Z. Zhu, Z. Meng and H.-Z. Geng, *Carbon*, 2021, **172**, 379–389.
14 S. Chen, L. Song, Z. Tao, X. Shao, Y. Huang, Q. Cui and X. Guo, *Org. Electron.*, 2014, **15**, 3654–3659.
15 M. H. Yousefi, A. Fallahzadeh, J. Saghaei and M. D. Darareh, *J. Disp. Technol.*, 2016, **12**, 1647–1651.
16 L. Lian, H. Wang, D. Dong and G. He, *J. Mater. Chem. C*, 2018, **6**, 9158–9165.
17 C. F. Guo and Z. Ren, *Mater. Today*, 2015, **18**, 143–154.
18 D. Li, W.-Y. Lai, F. Feng and W. Huang, *Adv. Mater. Interfaces*, 2021, **8**, 2100548.
19 B. Sun, R. Xu, X. Han, J. Xu, W. Hong, Y. Xu, Z. Fu, H. Zhu, X. Sun, J. Wang, P. Cui, J. Chang, J. Xiong and K. Qian, *npj Flexible Electron.*, 2022, **6**, 48.
20 X. Yin, J. Wang, A. Liu, W. Cai, L. Ying, X. He, Z. Tang and L. Hou, *Flexible Printed Electron.*, 2020, **5**, 014003.
21 L. Hu, H. S. Kim, J.-Y. Lee, P. Peumans and Y. Cui, *ACS Nano*, 2010, **4**, 2955–2963.
22 X. Dong, P. Shi, L. Sun, J. Li, F. Qin, S. Xiong, T. Liu, X. Jiang and Y. Zhou, *J. Mater. Chem. A*, 2019, **7**, 1989.
23 J. Kim, D. Ouyang, H. Lu, F. Ye, Y. Guo, N. Zhao and W. C. H. Choy, *Adv. Energy Mater.*, 2020, **10**, 1903919.
24 G.-R. Li and X.-P. Gao, *Adv. Mater.*, 2020, **32**, 1806478.
25 P. J. Maake, A. S. Bolokang, C. J. Arendse, V. Vohra, E. I. Iwuoha and D. E. Motaung, *Sol. Energy*, 2020, **207**, 347–366.
26 T. Tokuno, M. Nogi, M. Karakawa, J. Jiu, T. T. Nge, Y. Aso and K. Suganuma, *Nano Res.*, 2011, **4**, 1215–1222.
27 F. Wan, H. He, S. Zeng, J. Du, Z. Wang, H. Gu and J. Xiong, *Nanotechnology*, 2020, **31**, 325302.
28 S. Duan, L. Zhang, Z. Wang and C. Li, *RSC Adv.*, 2015, **5**, 95280–95286.
29 W.-H. Chen, F.-W. Li and G.-S. Liou, *Adv. Opt. Mater.*, 2019, **7**, 1900632.
30 X. Zhu, A. Guo, J. Xu and C. Kan, *CrystEngComm*, 2020, **22**, 8421–8429.
31 L. Shi, *Micro Nano Lett.*, 2023, **18**, 12151.
32 Y. Wang, Q. Chen, G. Zhang, C. Xiao, Y. Wei and W. Li, *ACS Appl. Mater. Interfaces*, 2022, **14**(4), 5699–5708.
33 D. Lee, D.-Y. Youn, Z. Luo and I.-D. Kim, *RSC Adv.*, 2016, **6**, 30331–30336.
34 J. A. Spechler, T.-W. Koh, J. T. Herb, B. P. Rand and C. B. Arnold, *Adv. Funct. Mater.*, 2015, **25**, 7428.
35 S. Yu, P. Yang, B. Wang, N. Zhang and C. Wu, *Mater. Lett.*, 2022, **328**, 133031.
36 Y. Xu, Z. Lin, W. Wei, Y. Hao, S. Liu, J. Ouyang and J. Chang, *Nano-Micro Lett.*, 2022, **14**, 117.
37 R. Miao, P. Li, W. Zhang, X. Feng, L. Qian, J. Fang, W. Song and W. Wang, *Adv. Mater. Interfaces*, 2022, **9**, 2101669.
38 N. Sharma, N. M Nair, G. Nagasarvari, D. Ray and P. Swaminathan, *Flexible Printed Electron.*, 2022, **7**, 014009.
39 N. M Nair, J. K. Pakkathillam, K. Kumar, K. Arunachalam, D. Ray and P. Swaminathan, *ACS Appl. Electron. Mater.*, 2020, **2**, 1000–1010.
40 H. Li, G. Ding and Z. Yang, *Micromachines*, 2019, **10**, 206.
41 L. Ju, Z. Wang, K. Sun, H. Peng, R. Fan and F. Qin, *Composites, Part A*, 2022, **153**, 106755.
42 D.-G. Kim, J. Kim, S.-B. Jung, Y.-S. Kim and J.-W. Kim, *Appl. Surf. Sci.*, 2016, **380**, 223–228.
43 N. M Nair, K. Daniel, S. C. Vadali, D. Ray and P. Swaminathan, *Flexible Printed Electron.*, 2019, **4**, 045001.
44 M. Li, W. Zuo, A. G. Ricciardulli, Y. Yang, Y. Liu, Q. Wang, K. Wang, G. Li, M. Saliba, D. D. Girolamo, A. Abate and Z. Wang, *Adv. Mater.*, 2020, **32**, 2003422.
45 J. Crêpellière, K. Menguelti, S. Wack, O. Bouton, M. Gérard, P. L. Popa, B. R. Pistillo, R. Leturcq and M. Michel, *ACS Appl. Nano Mater.*, 2021, **4**(2), 1126–1135.
46 X. Yuan, T.-X. Xiang, B. D. Anderson and E. J. Munson, *Mol. Pharmaceutics*, 2015, **12**(12), 4518–4528.
47 J. Jiu, T. Araki, J. Wang, M. Nogi, T. Sugahara, S. Nagao, H. Koga, K. Suganuma, E. Nakazawa, M. Hara, H. Uchida and K. Shinozaki, *J. Mater. Chem. A*, 2014, **2**(18), 6326–6330.
48 J. Jiu, T. Sugahara, M. Nogi and K. Suganuma, *J. Nanopart. Res.*, 2013, **15**(4), 1588.
49 X. Hu, J. He, L. Zhu, S. Machmudah, W. Diono, H. Kanda and M. Goto, *Polymers*, 2022, **14**(1), 89.
50 N. Li, X. Fan, K. Tang, X. Zheng, J. Liu and B. Wang, *Colloids Surf., B*, 2016, **140**, 287–296.
51 S. Jun, B.-K. Ju and J.-W. Kim, *Curr. Appl. Phys.*, 2017, **17**, 6–10.
52 S. Yu, X. Liu, P. Yang, L. Zhao, H. Dong, C. Wu, X. Li and J. Xiong, *Chem. Eng. J.*, 2022, **446**, 137481.
53 C. Chou, H. Liu and G. Liou, *RSC Adv.*, 2016, **6**, 61386–61392.
54 Y. Li, S. Chou, P. Huang, C. Xiao, X. Liu, Y. Xie, F. Zhao, Y. Huang, J. Feng, H. Zhong, H. Sun and Q. Pei, *Adv. Energy Mater.*, 2019, **31**, 1807516.
55 J. Jin, J. Li, Q. Tai, Y. Chen, D. D. Mishra, W. Deng, J. Xin, S. Guo, B. Xiao and X. Wang, *J. Power Sources*, 2021, **482**, 228953.
56 Z. Lu, Y. Lou, P. Ma, K. Zhu, S. Cong, C. Wang, X. Su and G. Zou, *Sol. RRL*, 2020, **4**(10), 2000320.
57 T. Y. Jin, W. Li, Y. Q. Li, Y. X. Luo, Y. Shen, L. P. Cheng and J. X. Tang, *Adv. Opt. Mater.*, 2018, **6**(24), 1801153.

58 Y. Jin, Y. Sun, K. Wang, Y. Chen, Z. Liang, Y. Xu and F. Xiao, *Nano Res.*, 2018, **11**, 1998–2011.
59 J. Wang, X. Liang, J. Xie, X. Yin, J. Chen, T. Gu, Y. Mo, J. Zhao, S. Liu, D. Yu, J. Zhang and L. Hou, *Nanomaterials*, 2022, **12**(22), 3987.
60 M. Kaltenbrunner, G. Adam, E. D. Głowacki, M. Drack, R. Schwödiauer, L. Leonat, D. H. Apaydin, H. Groiss, M. C. Scharber, M. S. White, N. S. Sariciftci and S. Bauer, *Nat. Mater.*, 2015, **14**, 1032–1039.